Characterization of type-II spontaneous parametric down-conversion in domain-engineered PPLN

Paulina S. Kuo[1,*], Thomas Gerrits[2], Varun Verma[2], Sae Woo Nam[2], Oliver Slattery[1], Lijun Ma[1] and Xiao Tang[1]

[1]Information Technology Laboratory, National Institute of Standards and Technology (NIST), 100 Bureau Drive, Gaithersburg, MD, USA 20899-8920

[2]Physical Measurement Laboratory, National Institute of Standards and Technology (NIST), 325 Broadway, Boulder, CO, USA 80305-3337

ABSTRACT

We characterize spontaneous parametric downconversion in a domain-engineered, type-II periodically poled lithium niobate (PPLN) crystal using seeded emission and single-photon techniques. Using continuous-wave (CW) pumping at 775 nm wavelength, the signal and idler are at 1532.5 nm and 1567.5 nm, respectively. The domain-engineered crystal simultaneously phasematches signal and idler pairs: [H(1532.5 nm), V(1567.5 nm)] and [V(1532.5 nm), H(1567.5 nm)]. We observe the tuning curves of these processes through difference-frequency generation and through CW fiber-assisted, single-photon spectroscopy. These measurements indicate good matching in amplitude and bandwidth of the two processes and that the crystal can in principle be used effectively to generate polarization-entangled photon pairs.

Keywords: quantum optics; nonlinear optics, parametric processes; polarization entangled pair source; spontaneous parametric downconversion; entanglement

1. INTRODUCTION

Entanglement is an important resource for quantum information systems. Entangled photon pairs generated by spontaneous parametric down-conversion (SPDC)[1,2] are an important tool for distributing entanglement between different systems and across large distances. By using quasi-phasematching (QPM)[3] in an SPDC crystal, a wide variety of nonlinear interactions with different wavelengths, bandwidths and polarization states can be obtained[4–6]. Photons generated near the 1550 nm telecom wavelength are very attractive for long-distance entanglement distribution over existing fiber links[5,7–9], which is important for the realization of practical quantum information networks.

We have designed a new scheme for generating polarization-entangled photons[10,11]. It is related to schemes that use two collinear processes in two consecutive, co-rotated crystals[12,13] and schemes that use two consecutive QPM periods[7,8]. These two schemes generate photon pairs of different polarizations but matched wavelengths. There is ambiguity where the pump photon is down-converted and which signal and idler pair is generated, and this ambiguity leads to quantum entanglement. In our scheme, instead of two discrete locations in the down-conversion crystal, we use a phase-modulated structure for the QPM grating that simultaneously phasematches the two type-II SPDC processes corresponding to $|H_{sig}V_{idl}\rangle$ and $|V_{sig}H_{idl}\rangle$[10,11]. This grating was fabricated in periodically poled lithium niobate (PPLN).

We have made progress in characterizing signal and idler generation in the domain-engineered crystal, but most of the measurements used seeding with classical light. It has been shown that there is a close relationship between stimulated and spontaneous emission of photon pairs, and that examining the stimulated emission processes can be a fast and effective means to gather information about the spontaneous emission processes[14]. Our measured seeded spectra showed good spectral matching between the two orthogonally polarized SPDC processes[11]. We recently have performed single-photon characterization of spontaneous photon pairs generated in the domain-engineered QPM crystal. Measurements were performed using fiber-assisted single-photon spectroscopy[15-17]. Here, we describe results of these single-photon characterizations and discuss implications for quantum entanglement. These single-photon measurements were in agreement with seeded spectral measurements.

*pkuo@nist.gov

2. THEORY

2.1 Engineering spontaneous parametric down-conversion

In the process of SPDC, a high-intensity pump at angular frequency ω_p incident on a second-order nonlinear optical crystal spontaneously splits into pairs of lower energy (longer wavelength) photons (signal, ω_s, and idler, ω_i) that are related to the pump photons by energy conservation ($\omega_p = \omega_s + \omega_i$). The spectrum of down-conversion is determined by

$$I_{SPDC} \propto \mathrm{sinc}^2\left(\frac{\Delta k L}{2}\right), \tag{1}$$

with $\mathrm{sinc}(x) = \sin(x)/x$, L is the length of the crystal, and for a collinear interaction,

$$\Delta k = k_p - k_s - k_i \pm \frac{2\pi}{\Lambda_{QPM}}, \tag{2}$$

where the wavevector $k_j = 2\pi n_j / \lambda_j$, n_j is the refractive index at wavelength λ_j and Λ_{QPM} is the period of the domain inversion pattern when quasi-phasematching is applied. Maximum conversion is obtained when $\Delta k = 0$. Since the indices of refraction depend on temperature, tuning of the wavelengths can be achieved by changing the crystal temperature.

A number of advanced techniques have been developed to modify the domain inversion pattern in order to engineer the frequency conversion spectrum. Here, we apply phase modulation of the QPM grating to produce multi-wavelength conversion[18,19]. In this technique, the domain positions within each period Λ_{QPM} are shifted with a shift characterized by a phase that ranges from 0 to 2π. The phase-shift pattern is periodic with period Λ_{ph}. If one wants to phasematch two processes with associated phase mismatches Δk_1 and Δk_2, then a phase-modulated grating can be designed such that

$$k_p - k_s - k_i = 2\pi\left(\frac{1}{\Lambda_{QPM}} + \frac{m_j}{\Lambda_{ph}}\right) = 0. \tag{3}$$

where m_j is the integer associated with process j (for the two-process example, $j = 1$ or 2). We have previously applied the phase-modulation technique to engineer dual-wavelength sum-frequency generation[20].

For type-II SPDC where we want to simultaneously generate $|H_{sig}V_{idl}\rangle$ and $|V_{sig}H_{idl}\rangle$, the two processes are

$$\begin{aligned}
\omega_p^{\mathrm{H}} &= \omega_s^{\mathrm{V}} + \omega_i^{\mathrm{H}} \\
\omega_p^{\mathrm{H}} &= \omega_s^{\mathrm{H}} + \omega_i^{\mathrm{V}}
\end{aligned}. \tag{4}$$

If we assign $m_1 = -1$ and $m_2 = 1$, then for 776 nm $\rightarrow$ 1535 nm + 1570 nm in MgO-doped PPLN[21], we calculate the required periods are $\Lambda_{\mathrm{QPM}} = 9.4$ µm and $\Lambda_{\mathrm{PM}} = 1.92$ mm when the crystal temperature is set to 70 °C.

3. DEVICE CHARACTERIZATION USING CLASSICAL LIGHT

We first characterized the phase-modulated QPM gratings using second-harmonic generation (SHG), sum- and difference-frequency generation (SFG and DFG). In the design of the crystal using the theoretical refractive indices[21], the crystal temperature where the wavelengths of the $|H_{sig}V_{idl}\rangle$ and $|V_{sig}H_{idl}\rangle$ are matched was 70 °C. However, initial measurements of the actual crystal showed that the real temperature was higher. Instead of operating near 70 °C, the PPLN device needed to be operated at 140 °C or higher in order to phasematch the pump wavelength near 775 nm, and signal and idler near 1550 nm. Figure 1a shows the measured SHG tuning curve for a phase-modulated QPM grating at 140 °C. Two peaks are clearly visible, indicating that two nonlinear processes are simultaneously phasematched.
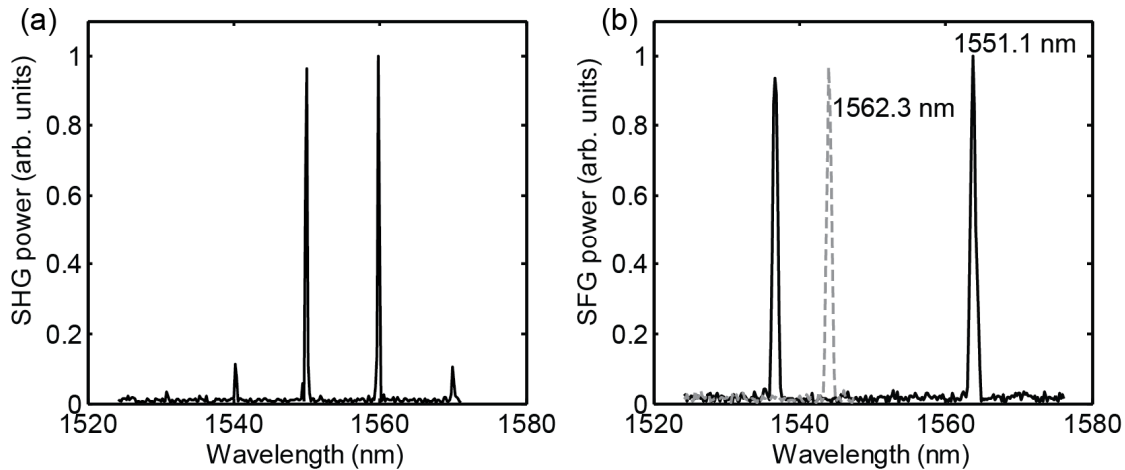
Figure 1. Measured (a) second-harmonic generation and (b) sum-frequency generation tuning curves at T=140 °C. For SHG, the fundamental beam is polarized at 45° to the crystal axes for the type-II interaction. For SFG, the vertically polarized beam is fixed to 1551.1 nm (solid) or 1562.3 nm (dashed) while the horizontally polarized beam is swept in wavelength. For the solid curve, both peaks are visible, while for the dashed curve, the second peak fell outside the tuning range of the laser around 1517 nm. The powers are given in arbitrary units (arb. units) with the maximum powers scaled to 1.
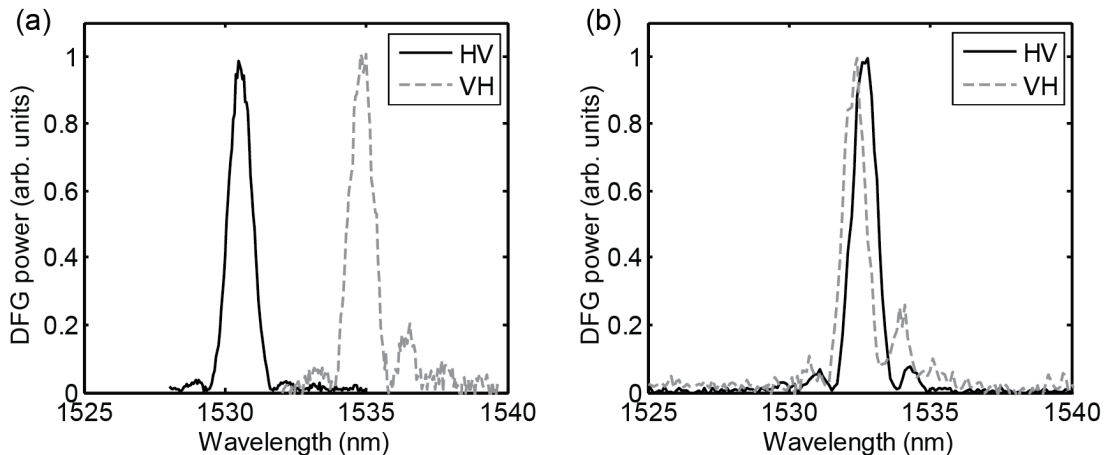

Figure 2. Difference-frequency generation spectra at two crystal temperatures, (a) 140 °C and (b) 143.5 °C. The horizontally polarized pump is fixed to 774.8 nm. The HV curve represents the state $|H_{sig}V_{idl}\rangle$; that is, the signal beam near 1530 nm is horizontally polarized while the corresponding idler near 1570 nm is vertically polarized. The maximum power is scaled to 1 for each trace.

We also observed SFG in the phase-modulated PPLN gratings. We used two continuous-wave, tunable, C-band, external cavity diode lasers. The two lasers were combined using a fiber beam combiner to ensure perfect co-alignment, and the beams were focused into the PPLN grating. Figure 1b shows observed sum-frequency tuning curves for the same grating at 140 °C. Since the nonlinear interaction is type-II, the two beams near 1550 nm must be orthogonally polarized. We fixed the vertically polarized beam to 1551.1 nm or 1562.3 nm wavelength and swept the horizontally polarized beam. The two traces in Fig. 1b are labeled by the wavelength of the fixed laser. Increasing the wavelength of the vertically polarized beam causes the tuning curve for the horizontal polarization to shift to shorter wavelengths.

After determining the proper operating temperature through the SHG and SFG measurements, we performed DFG using the phase-modulated QPM gratings. We used a fixed-wavelength, distributed feedback diode laser at 774.8 nm and a tunable external cavity diode laser near 1550 nm. A Glan-Thompson polarizer after the PPLN was used to reject the signal beam and transmit the generated difference-frequency (DF) beam. A 1550 nm dichroic edge filter was also used to improve separation of the signal and DF beams. The DF beam was detected with an InGaAs detector. Results of DFG measurements are presented in Fig. 2. At 140 °C, the spectrum for the $|H_{sig}V_{idl}\rangle$ process does not overlap with the

spectrum for the $|V_{sig}H_{idl}\rangle$ process. By increasing the temperature to 143.5 °C, we achieve good spectral overlap where $\lambda(H_{sig}) = \lambda(V_{sig}) = 1532.5$ nm. We also observed that the spectral bandwidths are nearly equal, which is important for preserving entanglement and not using additional filters.

It has been recently argued that such characterization with classical light is a fast and effective technique to infer information about the associated spontaneous emission processes that are later used for quantum entanglement[14]. Indeed, our seeded emission measurements inform us of the proper operating temperature and show that the spectra of the two processes are similar in bandwidth and in side-lobe structure. However, single-photon characterizations are still very important as ultimately, single-photon measurements are needed to observe quantum behavior.

4.   OBSERVATION OF SPONTANEOUS EMISSION SPECTRA

4.1 Fiber-assisted, single-photon spectroscopy

Superconducting nanowire single photon detectors (SNSPDs) have remarkably high detection efficiency (up to 93% efficiency) and very small timing jitter (~100 ps)[22]. This fine temporal resolution can be translated to spectral resolution by incorporating a dispersive medium so that different wavelength components of the test light arrive at the detector at different times. This is the underlying principle of fiber-assisted, single-photon spectroscopy[15-17], where the dispersion is provided by a long length of optical fiber or a more compact fiber dispersion compensation module (DCM).

We first characterized the dispersion produced by the DCM. Figure 3a shows the measured relative time delay of different spectral components passing through the DCM. The slope of this data with respect to wavelength gives the dispersion, which is shown in Fig. 3b. At 1550 nm wavelength, the DCM produces -1.0 ns/nm dispersion. The negative sign of the dispersion indicates that longer wavelengths lead the shorter wavelengths.

Figure 4 shows the experimental setup. The domain-engineered PPLN crystal is pumped with a continuous-wave 775-nm wavelength laser that has a linewidth below 200 kHz. After the PPLN, the pump is filtered out with a dichroic mirror and the orthogonally polarized signal and idler photons are sent to a half-wave plate (HWP) and polarization beam splitter (PBS). For most measurements, the HWP is removed altogether or positioned to have no effect so that the horizontally polarized photons are transmitted and the vertically polarized photons are reflected by the PBS. For certain measurements, the HWP is positioned to produce 45° of polarization rotation, which effectively makes the PBS a non-polarizing beam splitter. After the beam splitter, both beams are coupled into optical fibers. We did not fully optimize the collection efficiency, which was around 5% to 10%. Since the fiber-assisted spectroscopy measurement requires clicks from both arms, mismatched collection efficiencies do not distort the spectral measurement but they do change the overall coincidence count rate. We incorporated DCMs into one or both of the arms after the beam splitter. With a single DCM, the undispersed arm after the PBS serves as a trigger while the other arm is dispersed by roughly 1 ns/nm. When two DCMs are used, the signal-idler dispersion is doubled at the expense of coincident count rate reduction since each DCM has about 4 dB loss. The photons were detected by SNSPDs and the arrival times analyzed with time-tagging electronics.
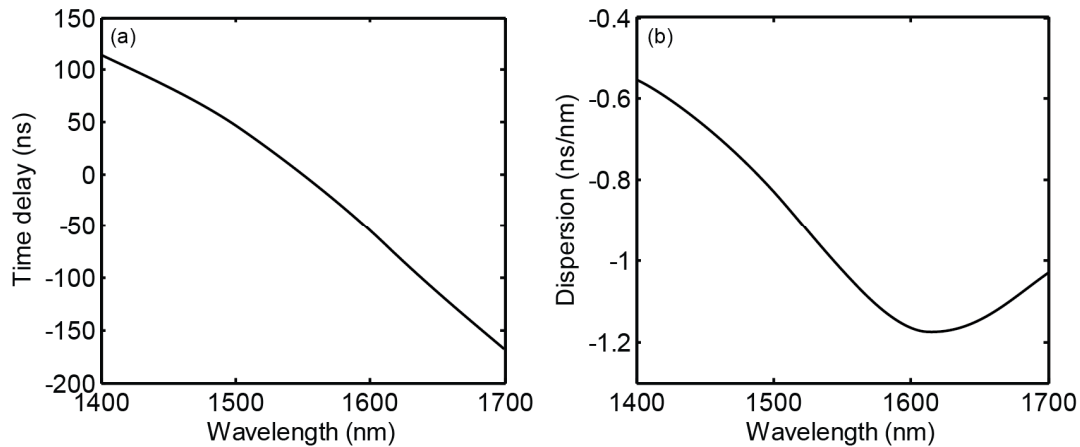

Figure 3. (a) Relative time delay of different wavelengths passing through the dispersion compensation module. (b) Dispersion produced by the DCM. At 1550 nm, the dispersion is -1 ns/nm.
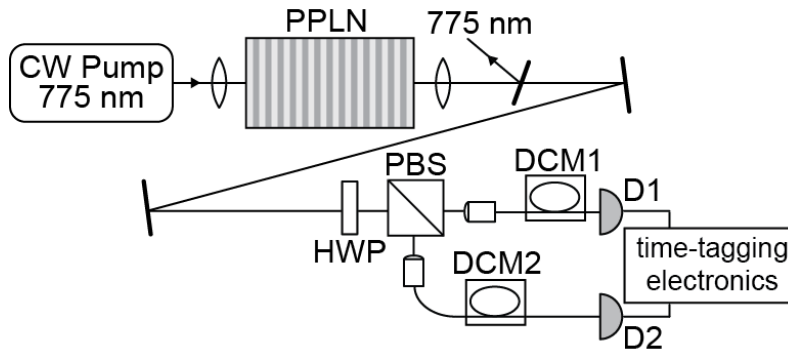
Figure 4. Sketch of experimental setup. The PPLN crystal is pumped by a CW 775 nm laser. Horizontally and vertically polarized photons near 1550 nm are produced by SPDC. The down-converted photons are incident on a beam splitter (polarizing beam splitter when the HWP is removed, and non-polarized beam splitter when the half-wave plate (HWP) rotates polarizations by 45°) and then coupled into optical fibers. The light is dispersed with dispersion compensation modules DCM1 and/or DCM2 then detected by SNSPDs. Arrival times are logged using time-tagging electronics.
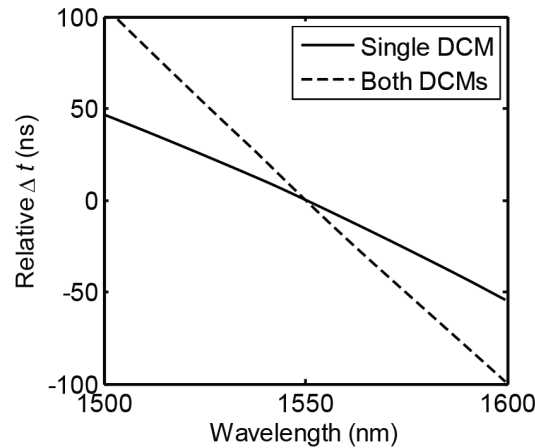

Figure 5. Map between wavelength and relative difference in arrival times of photons at D1 and D2 (Δt) for single DCM in only one arm of the experiment, and DCMs in both arms of the experiment (as sketched in Fig. 4). A larger spread in arrival times is obtained with both DCMs than with a single DCM. We set $\Delta t = 0$ for 1550 nm, which is $2\lambda_{pump}$, where the signal and idler wavelengths would be degenerate.

Using the dispersion data in Fig. 3 and the fact that the pump is narrowband, we can map the difference in arrival times of photons at D1 and D2 (in Fig. 4) to the signal-idler pair that produced the pair of clicks. This mapping is shown in Fig. 5. In Fig. 5, we see that when using two DCMs produces roughly twice more temporal spread for the same signal-idler wavelengths as one DCM. The y-axis of this figure is given in relative delay, with Δt set to 0 at 1550 nm wavelength. We also note that each DCM produces 30 µs of fixed delay. We calibrate the delay caused by experimental path imbalances by examining data where the HWP and PBS together act as a non-polarizing beam splitter and look for symmetry when the measured data are reflected about $2\lambda_{pump}$.

4.2 Measured single-photon spectra

Spectra taken using a single DCM are shown in Fig. 6. The PPLN temperature was 138 °C. We used 1 minute integration time for this data with 3 mW CW pump power incident on the PPLN crystal. The x-axis represents the wavelength of the H-polarized photons. In Fig. 6a, we show the effect of inserting the HWP before the PBS. Without the HWP, the H-polarized photons are sent to D1 and the V-polarized photons are sent to D2 (with DCM2 in the V-arm to disperse the wavelengths and no DCM in the H-arm). Two peaks are visible, which correspond to the two SPDC processes $|H_{sig}V_{idl}\rangle$ and $|V_{sig}H_{idl}\rangle$. When the HWP is inserted before the PBS, all four possible signal and idler photons are sent to both arms. The measurement records coincidences in D1 and D2, which reflect the pairs of photons generated by SPDC. Since now the H-polarized and the V-polarized photons pass through DCM2, we see twice the number of

peaks. Specifically, the peak at 1529 nm is the same process that corresponds to the peak at 1571 nm (and similarly for the peaks at 1536 nm and 1564 nm). In Fig. 6b, we compare spectra measured with only DCM1 in the H-arm or only DCM2 in the V-arm. We see that the spectrometer works well in either configuration; the spectra show excellent agreement especially in the fine structure of the side lobes.
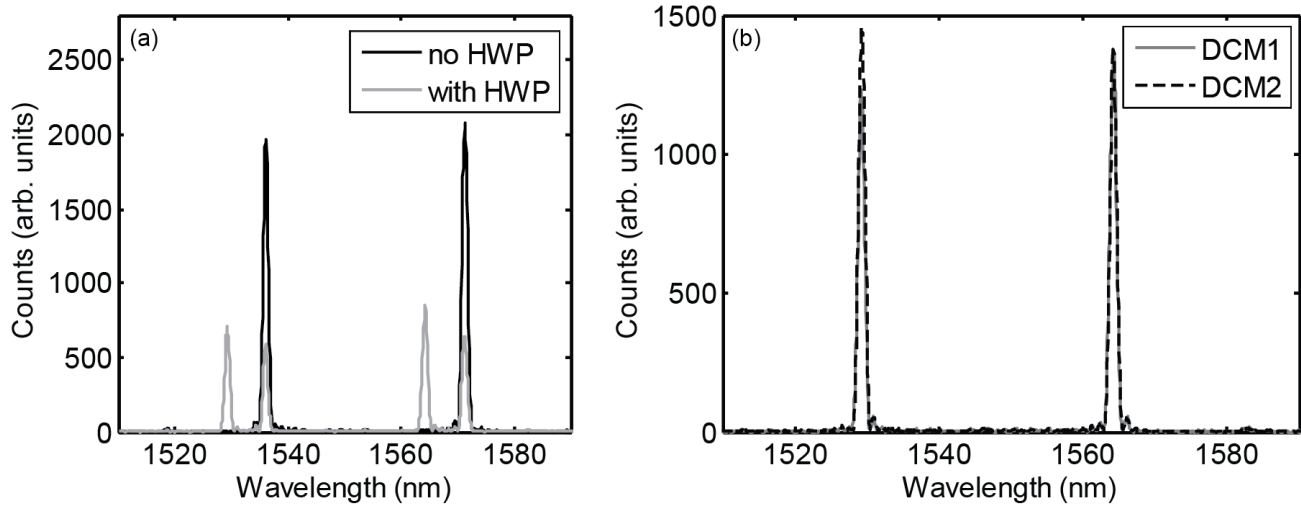

Figure 6. (a) SPDC spectra measured using only DCM2 with and without the half-wave plate. The HWP sends all four photons to both arms, which leads to the apparent splitting of the peaks. (b) SPDC spectra measured without the HWP and with a single DCM in the experiment in the H-arm (DCM1) or the V-arm (DCM2). There is excellent agreement in the observed spectra.
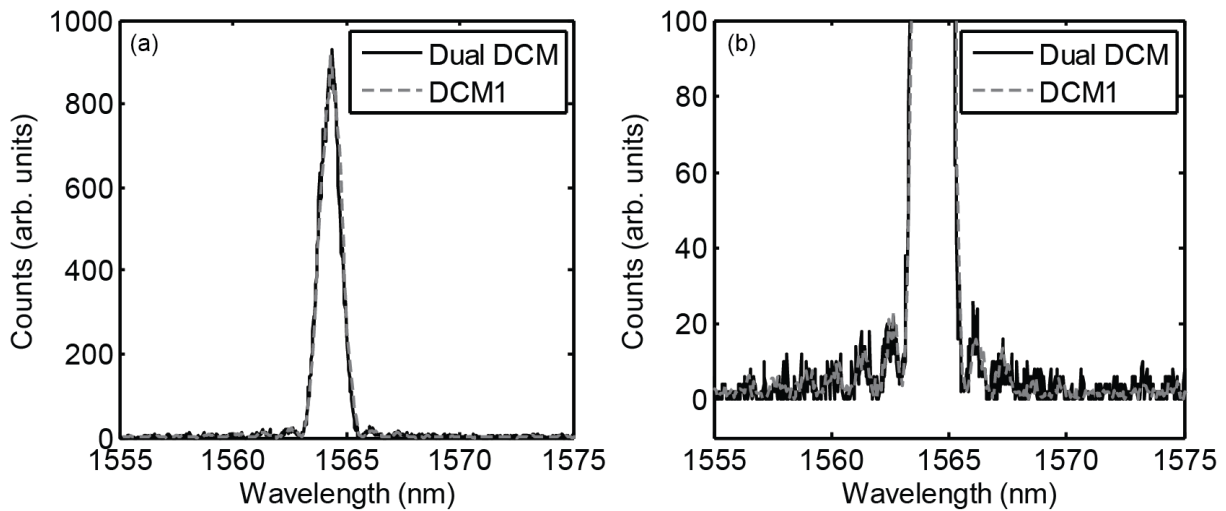

Figure 7. Comparison of spectra measured with DCMs in both arms after the PBS and with DCM1 in the H-arm only. The PPLN temperature is set to 138 °C. (b) is a zoom in of (a). Peaks are scaled to equal heights and counts are shown in arbitrary units. There is agreement in the spectra, but the data using dual DCMs show worse signal-to-noise ratio.

We also measured SPDC spectra using DCMs in both arms of the experimental setup. Having two DCMs compared to a single DCM in the setup caused the coincidence rate to drop by a factor of 10. To compensate for the lower count rates, we integrated for 3 minutes instead of the 1 minute used for single DCM measurements. Figure 7 shows a comparison of the spectra measured with dual and single DCM. In these measurements, the PPLN temperature was at 138 °C. We focus on the peak near 1564 nm. We scaled the data to have equal maxima and zoom in to examine the side lobes in Fig. 7b. There is good agreement in the two traces. Even though the dual DCM measurement had three times longer integration time, because of the low coincidence count rate, the signal-to-noise rate was worse than the DCM1 measurement.
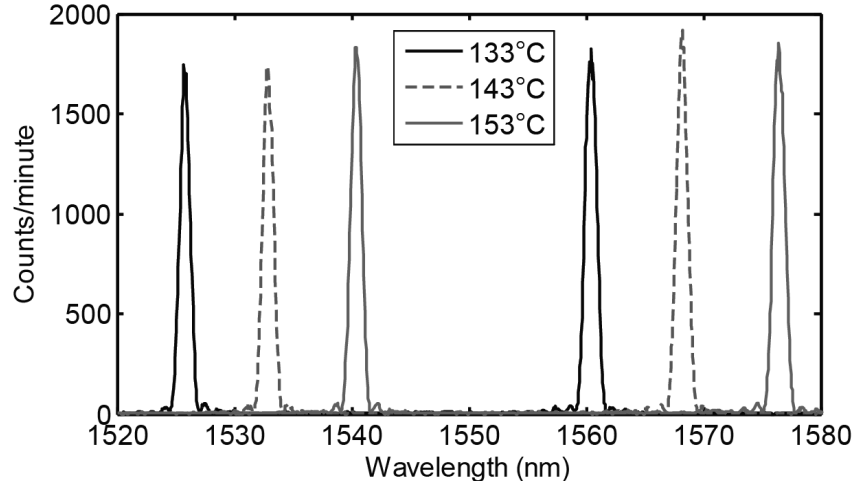
Figure 8. Temperature tuning of the domain-engineered PPLN crystal. Each trace is measured with no HWP, DCM1 in the setup, and an integration time of one minute.

Figure 8 illustrates temperature tuning of SPDC produced by the domain-engineered PPLN crystal. The spectra were measured with a single DCM in the setup (DCM1), no HWP and one minute integration time. At PPLN temperature of 143°C, we achieve $\lambda(H_{sig}) = \lambda(V_{sig})$ and $\lambda(V_{idl}) = \lambda(H_{idl})$ and the two processes $|H_{sig}V_{idl}\rangle$ and $|V_{sig}H_{idl}\rangle$ become indistinguishable in wavelength. At this temperature, the two peaks become equally spaced about $2\lambda_{pump} = 1550$ nm. In contrast, the spectrum measured with the HWP in Fig. 6a clearly show that at 138 °C, $\lambda(H_{sig}) \neq \lambda(V_{sig})$ and $\lambda(V_{idl}) \neq \lambda(H_{idl})$. The single-photon spectra shown in Figs. 6 through 8 are in good agreement with seeded spectra (Fig. 2).

5. DISCUSSION

We characterized the down-conversion spectra of the domain-engineering PPLN crystal at both the classical and single-photon light levels. There was good agreement between the single-photon and seeded measurement results. Also, the spectra agree well with theoretical predictions based on the QPM domain design. The 35 nm spacing between the two peaks was as designed, and the observed peaks had sinc²-like shapes. The only design discrepancy was the operating temperature, which was about 70 °C higher than theoretically predicted. The phase-modulated QPM structure also produced small satellite peaks around 1500 nm and 1600 nm in wavelength, just outside the range of the spectrum plotted in Fig. 6b. These satellite peaks were both predicted theoretically and observed experimentally.

This technique to measure single-photon SPDC spectra, fiber-assisted single-photon spectroscopy, is a very powerful and fast way to characterize SPDC sources. We show here that it works well for CW-pumped SPDC while pulsed pumping was shown previously[15-17]. We easily acquired spectra spanning ~100 nm with 1 minute integration, which is arguably faster than using a single-photon detector and scanning the spectrum with a monochromator. In fact, our difference-frequency generation measurements (performed by scanning the laser wavelength and recording the InGaAs photodiode response) took about 5 minutes to acquire, yet the DFG spectra (Fig. 2) seem noisier than the single-photon spectra with 1 minute acquisition time shown in Fig. 8. The advantages of the fiber-assisted single-photon spectral measurements can be attributed to the high performance of the SNSPDs and the fast data collection using the time-tagging electronics. The DFG spectra were taken using a chopper, lock-in amplifier and battery-powered InGaAs biased photodiode. This classical light measurement has a much higher noise floor than measurements using SNSPDs.

In our future work, we plan to measure the entanglement visibility of our source. Good entanglement requires the two processes be indistinguishable. The observed spectra show the point where the wavelengths of the two processes are matched (T=143 °C). The amplitudes and widths of the two peaks are also nearly the same. We must implement temporal compensation to erase the effects of the PPLN birefringence, which causes the different polarizations to walk-off in time and become distinguishable by their relative arrival times[23]. Our measurements here indicate that the domain-engineering PPLN SPDC source has the potential to produce high-quality quantum entanglement.

6. CONCLUSION

We have designed and characterized an engineered nonlinear crystal for use as a source of polarization-entangled photon pairs. The PPLN crystal uses a phase-modulated QPM grating design to phasematch the generation of $|H_{sig}V_{idl}\rangle$ and $|V_{sig}H_{idl}\rangle$ states in a single crystal. We performed stimulated and spontaneous emission down-conversion spectral measurements on the crystal and observed the two simultaneous processes, which operate at 775 nm $\rightarrow$ 1532.5 nm + 1567.5 nm when the wavelengths are matched. We demonstrate that CW-pumped SPDC can be effectively characterized by fiber-assisted single-photon spectroscopy. These results are promising signs that our crystal can perform well in quantum entanglement applications.

REFERENCES

[1] Kwiat, P. G., Mattle, K., Weinfurter, H., Zeilinger, A., Sergienko, A. V., and Shih, Y., "New high-intensity source of polarization-entangled photon pairs," Phys. Rev. Lett. 75(24), 4337-4341 (1995).

[2] Kurtsiefer, C., Oberparleiter, M., and Weinfurter, H., "High-efficiency entangled photon pair collection in type-II parametric fluorescence," Phys. Rev. A 64, 023802 (2001).

[3] Fejer, M. M., Magel, G. A., Jundt, D. H., and Byer, R. L., "Quasi-phase-matched second harmonic generation: tuning and tolerances," IEEE J. Quantum Electron. 28(11), 2631-2654 (1992).

[4] Tanzilli, S., De Riedmatten, H., Tittel, W., Zbinden, H., Baldi, P., De Micheli, M., Ostrowsky, D. B., and Gisin, N., "Highly efficient photon-pair source using periodically poled lithium niobate waveguide," Electron. Lett. 37(1), 26-28 (2001).

[5] Da Cunha Pereira M., Becerra, F. E., Glebov, B. L., Fan, J., Nam, S., and Migdall, A., "Demonstrating highly symmetric single-mode, single-photon heralding efficiency in spontaneous parametric downconversion," Opt. Lett. 38(10), 1609-1611 (2013).

[6] Tanzilli, S., Tittel, W., Halder, M., Alibart, O., Baldi, P., Gisin, N., and Zbinden, H., "A photonic quantum information interface," Nature 437, 116-120 (2005).

[7] Suhara, T., Nakaya, G., Kawashima, J, and Fujimura, M., "Quasi-phase-matched waveguide devices for generation of postselection-free polarization-entangled twin photons," IEEE Photon. Technol. Lett. 21(15), 1096-1098 (2009).

[8] Ueno, W., Kaneda, F., Suzuki, H., Nagano, S., Syouji, A., Shimizu, R., Suizu, K., and Edamatsu, K., "Entangled photon generation in two-period quasi-phase-matched parametric down-conversion," Opt. Express 20(5), 5508-5517 (2012).

[9] Herrmann, H., Yang, X., Thomas, A., Poppe, A., Sohler, W., and Silberhorn, C., "Post-selection free, integrated optical source of non-degenerate, polarization entangled photon pairs," Opt. Express 21(23), 27981-27991 (2013).

[10] Kuo, P. S., Pelc, J. S., Slattery, O., Kim, Y.-S., and Tang, X., "Entangled photon generation in a phase-modulated, quasi-phasematched crystal," Proc. SPIE 8875, 887508 (2013).

[11] Kuo, P. S., Pelc, J. S., Slattery, O., Ma, L., and Tang, X., "Domain-engineered PPLN for entangled photon generation and other quantum information applications," Proc. SPIE 9136, 913603 (2014).

[12] Trojek, P., and Weinfurter, H., "Collinear source of polarization-entangled photon pairs at nondegenerate wavelengths," Appl. Phys. Lett. 92, 211103 (2008).

[13] Steinlechner, F., Trojek, P., Jofre, M., Weier, H., Perez, D., Jennewein, T., Ursin, R., Rarity, J., Mitchell, M. W., Torres, J. P., Weinfurter, H., and Pruneri, V., "A high-brightness source of polarization-entangled photons optimized for applications in free space," Opt. Express 20(9), 9640-9649 (2012).

[14] Liscidini, M., and Sipe, J. E., "Stimulated Emission Tomography," Phys. Rev. Lett. 111, 193602 (2013).

[15] Avenhaus, M., Eckstein, A., Mosley, P. J., and Silberhorn, C., "Fiber-assisted single-photon spectrograph," Opt. Lett. 34(18), 2873-2875 (2009).

[16] Gerrits, T., Stevens, M. J., Baek, B., Calkins, B., Lita, A., Glancy, S., Knill, E., Nam, S. W., Mirin, R. P., Hadfield, R. H., Bennink, R. S., Grice, W. P., Dorenbos, S., Zijlstra, T., Klapwijk, T., and Zwiller, V., "Generation of degenerate, factorizable, pulsed squeezed light at telecom wavelengths," Opt. Express 19(24), 24434 (2011).

[17] Gerrits, T., Marsili, F., Verma, V. B., Shalm, L. K., Shaw, M., Mirin, R. P., and Nam, S. W., "Spectral correlation measurements at the Hong-Ou-Mandel interference dip," Phys. Rev. A 91, 013830 (2015).

[18] Asobe, M., Tadanaga, O., Miyazawa, H., Nishida, Y. and Suzuki, H., "Multiple quasi-phase-matched LiNbO$_3$ wavelength converter with a continuously phase-modulated domain structure," Opt. Lett. 28(7), 558-560 (2003).

[19] Asobe, M., Tadanaga, O., Miyazawa, H., Nishida, Y., and Suzuki, H., "Multiple quasi-phase-matched device using continuous phase modulation of $\chi^{(2)}$ grating and its application to variable wavelength conversion," IEEE. J. Quantum Electron. 41(12), 1540-1547 (2005).

[20] Pelc, J. S., Kuo, P. S., Slattery, O., Ma, L., Tang, X., and Fejer, M. M., "Dual-channel, single-photon upconversion detector at 1.3 μm," Opt. Express 20(17), 19075-19087 (2012).

[21] Gayer, O., Sacks, Z., Galun, E., and Arie, A., "Temperature and wavelength dependent refractive index equations for MgO-doped congruent and stoichiometric $LiNbO_3$," Appl. Phys. B 91, 343-348 (2008).

[22] Marsili, F., Verma, V. B., Stern, J. A., Harrington, S., Lita, A. E., Gerrits, T., Vayshenker, I., Baek, B., Shaw, M. D., Mirin, R. P., and Nam, S. W., "Detecting single infrared photons with 93% system efficiency," Nat. Photon. 7, 210-214 (2013).

[23] Shih, Y., "Entangled photons," IEEE J. Sel. Topics Quantum Electron. 9(6), 1455-1467 (2003).